Supporting Information

Patten and Ali 10.1073/pnas.0811171106

Materials and Methods

Preparation. Wild-type Zebrafish (*Danio rerio*) embryos were raised at 28.5 °C, and collected and staged as previously described (1). All procedures were carried out in compliance with the guidelines stipulated by the Canadian Council for Animal Care and the University of Alberta. Zebrafish (48 h postfertilization) were anesthetized in 0.02% tricaine (MS-222) (Sigma-Aldrich) and dissected. Briefly, the entire hindbrain was exposed after removing the forebrain and rostral structures, but leaving the spinal cord and trunk intact.

Electrophysiology. Preparations were moved to the recording set-up, and the chamber was continuously perfused at room temperature (20–24 °C) with an aerated recording solution that contained 15 μM D-tubocurarine (Sigma-Aldrich) to paralyze the preparations, but lacked tricaine. The miniature excitatory postsynaptic currents (mEPSC) recording solution contained (in mM) 134 NaCl, 2.9 KCl, 2.1 $CaCl_2$, 1.2 $MgCl_2$, 10 Hepes, 10 glucose and 0.001 TTX, with the osmolarity adjusted to 280 mOsm, pH 7.8. Whole-cell recordings were obtained from Mauthner neurons located in rhombomere 4. These cells were easily identified under Nomarski differential interference contrast (DIC) optics based on their morphology and location in the hindbrain. Patch-clamp electrodes were pulled from borosilicate glass and when filled with a Cs-gluconate solution and had resistances of 3.5–5 MΩ. The Cs-gluconate intracellular solution was composed of (in mM) 115 Cs-gluconate, 15 CsCl, 2 $MgCl_2$, 10 Hepes, 10 EGTA, and 4 Na_2ATP, osmolarity adjusted to 290 mOsm, pH 7.2. Chemical depolarization of the Mauthner cell was induced by a 10-min bath application of a 5 mM K^+ depolarizing medium that contained (in mM): 130 NaCl, 5 KCl, 2.1 $CaCl_2$, 0.3 $MgCl_2$, 10 Hepes, 10 glucose, and 1 TEA, osmolarity adjusted to 280 mOsm, pH 7.8. Postsynaptic depolarization of the Mauthner cell was induced by applying a series of 10 voltage steps from −80 to + 20 mV, lasting 3 s, given at an interpulse interval of 6 s (2).

Whole-cell currents were recorded by using an Axopatch 200B amplifier (MDS Analytical Technologies), then low-pass filtered at 10 kHz (−3 dB), and digitized at 50 kHz. Synaptic currents were recorded at a holding potential of −60 mV. Immediately after establishment of the whole-cell recording mode, series resistance was compensated by 70–85%, using the amplifier's compensation circuitry. Series resistance was monitored throughout the recording, which was abandoned if the resistance changed by >15%.

Analysis of mEPSCs. Synaptic activity was monitored using pClamp 8.1 software (MDS Analytical Technologies). Synaptic events were detected (using the template function for events >2.5 SDs above the basal noise), and analyzed with Axograph X (MDS Analytical Technologies). The software detected all events that could be recognized visually. All events were then inspected visually, and those with uneven baselines or overlaying events (<5%) were discarded. The decay time course was analyzed over the first 30 ms, and was fit with a sum of exponential curves. Averages of these events were best fit with one exponential curve. The rise times were defined as the time from 20 to 80% of the mEPSC amplitude. The rectification index was defined as peak current amplitude at a holding potential of +40 mV divided by that at −60 mV.

All data values are given as means ± SEM. Significance was determined by using paired *t* tests, 1-way ANOVA, and Fisher LSD for normally distributed, equal variance data. Kruskal–Wallis ANOVA and Dunn's method of comparison were used for nonnormal distributions.

Nonstationary Fluctuation Analysis (NSFA). We performed NSFA to estimate the single-channel current (i) and the available number of channels (N) (3). The mEPSCs were aligned on their rise time, and events with obvious artifacts were manually discarded. NSFA was performed on the deactivation phase of the responses. The averaged current and variance over time were computerized by using Axograph 4.6 software (MDS Analytical Technologies). Between 40 and 100 traces per patch were obtained for analysis.

The variance (σ^2) was plotted against the mean current (I) and the data points were fitted with the following parabolic function (3).

$$\sigma^2(I) = iI - I^2/N + {\sigma_b}^2$$

where i is the elementary current of the receptor channel, N is the total number of available AMPA receptors (Rs) at the synapse, and ${\sigma_b}^2$ is the variance of the background noise. The conductance value (γ) for each channel was then calculated by the equation $i/(V_m - E_{rev})$, with $V_m = -60$ mV and $E_{rev} = 0$ mV.

Immunohistochemical Procedures. Zebrafish 2 days post fertilization (dpf) embryos were fixed in 2% paraformaldehyde for 1–2 h. Tissues were washed several times in PBS and permeabilized for 30 min in 4% Triton-X 100 containing 2% BSA and 10% goat serum. After permeabilization, tissues were incubated in the primary antibodies 3A10 (1:250; Developmental Studies Hybridoma Bank), PKCα, βII or γ (1:500; Santa Cruz Biotechnology) for 48 h at 4 °C on a shaker. Tissues were washed several times in PBS over a 24-h period, and then incubated in the secondary antibodies conjugated with Cy3 or Alexa 488 (1:2,000; Molecular Probes) for 4–6 h at room temperature. Animals were washed in PBS several times, deyolked, cleared in 70% glycerol, and mounted. Z-stack images were photographed by using a Zeiss LSM 510 confocal microscope under a 20× objective, and were compiled by using Zeiss LSM Image Browser software.

Western Blot Analysis. Zebrafish brains were incubated with or without the PKCγ inhibitor peptide (γV5-3) (1 μM in 200 μL PBS for 10 min), followed by 5-min incubation with or without 5 nM phorbol myristate acetate (PMA). The incubation was stopped by snap freezing the samples on dry ice. Samples were then homogenized in a homogenization buffer (in mM: sucrose, 250; EDTA, 1; Tris, 30, pH 7.4) containing protease inhibitors (3 mM PMSF, 40 μM leupeptin, 4 μM pepstatin A, 0.4 mg/mL aprotinin), and centrifuged at 1,000 × g at 4 °C for 15 min. Supernatants were collected and centrifuged at 10,000 × g at 4 °C for 15 min. Then, the supernatants were collected, and pellets were resuspended in homogenization buffer supplemented with 1% SDS (V/V), incubated on ice for 30 min, and spun at 100,000 × g at 4 °C for 30 min. The supernatants were removed to quantify the protein content, and the pellets were discarded. Protein quantification was performed by using the BCA protein assay kit (Pierce), and 10 μg of zebrafish homogenate was loaded per lane. Samples were subjected to SDS/PAGE (10%), and transferred to nitrocellulose membranes by using a semidry transfer apparatus (Bio-Rad). Membranes were blocked in blocking buffer (5% skim milk powder, 0.1% Tween-20 in TBS) for 1 h at room temperature, and incubated in primary antibodies anti-PKCγ (1:1,000; Santa Cruz Biotech-

nology) and anti-acetylated tubulin (1:20,000; Sigma-Aldrich) overnight at 4 °C. Membranes were washed several times in TBS-T and incubated in secondary antibodies coupled to horse radish peroxidase (HRP; 1:40,000 goat anti rabbit IgG and HRP; 1:100,000 goat anti mouse IgG; Santa Cruz Biotechnology) for 1 h at room temperature on a shaker. Signals were detected with enhanced chemiluminescence (SuperSignal West Pico; Pierce), and developed on X-ray film. Immunoreactive bands were quantified densitometry (Adobe Photoshop).

Drugs. Strychnine (5 μM), picrotoxin (100 μM), APV (50 μM), Pentobarbital (100 μM), 1-Napthylacetylspermine (NASPM; 10 μM) and BAPTA (5 mM) were obtained from Sigma-Aldrich. PMA (100 nM) was obtained from Alexis Biochemical. Bisindolymaleimide I (BIS I; 500 nM) and Latrunculin B (5 μM) were purchased from Calbiochem. Tetrodotoxin (TTX; 1 μM) and the peptides pep2m, pep4c, pep2-EVKI, and pep2-SVKE were purchased from Tocris. The PKCγ inhibitor γV5–3 (γPKC antagonist; 10 nM) and its control peptide (C1; 10 nM) were gifts from KAI pharmaceuticals. The peptide competes with activated PKCγ for binding to the isozyme-specific docking proteins, receptors for activated C kinase. This strategy prevents PKC isozyme translocation and functioning in an isozyme-specific manner (1, 4). Active PKCγ (10 ng/uL) was obtained from Millipore. Tetanus toxin light chain (TeTx; 200 nM) was purchased from List Biological Laboratories.

1. Kimmel CB, Hatta K, Metcalfe WK (1990) Early axonal contacts during development of an identified dendrite in the brain of the zebrafish. *Neuron* 4:535–545.
2. Baxter AW, Wyllie DJ (2006) Phosphatidylinositol 3 kinase activation and AMPA receptor subunit trafficking underlie the potentiation of miniature EPSC amplitudes triggered by the activation of L-type calcium channels. *J Neurosci* 26:5456–5469.
3. Sigworth FJ (1980) The variance of sodium current fluctuations at the node of Ranvier. *J Physiol* 307:97–129.
4. Abeliovich A, et al. (1993) PKC gamma mutant mice exhibit mild deficits in spatial and contextual learning. *Cell* 75:1263–1271.

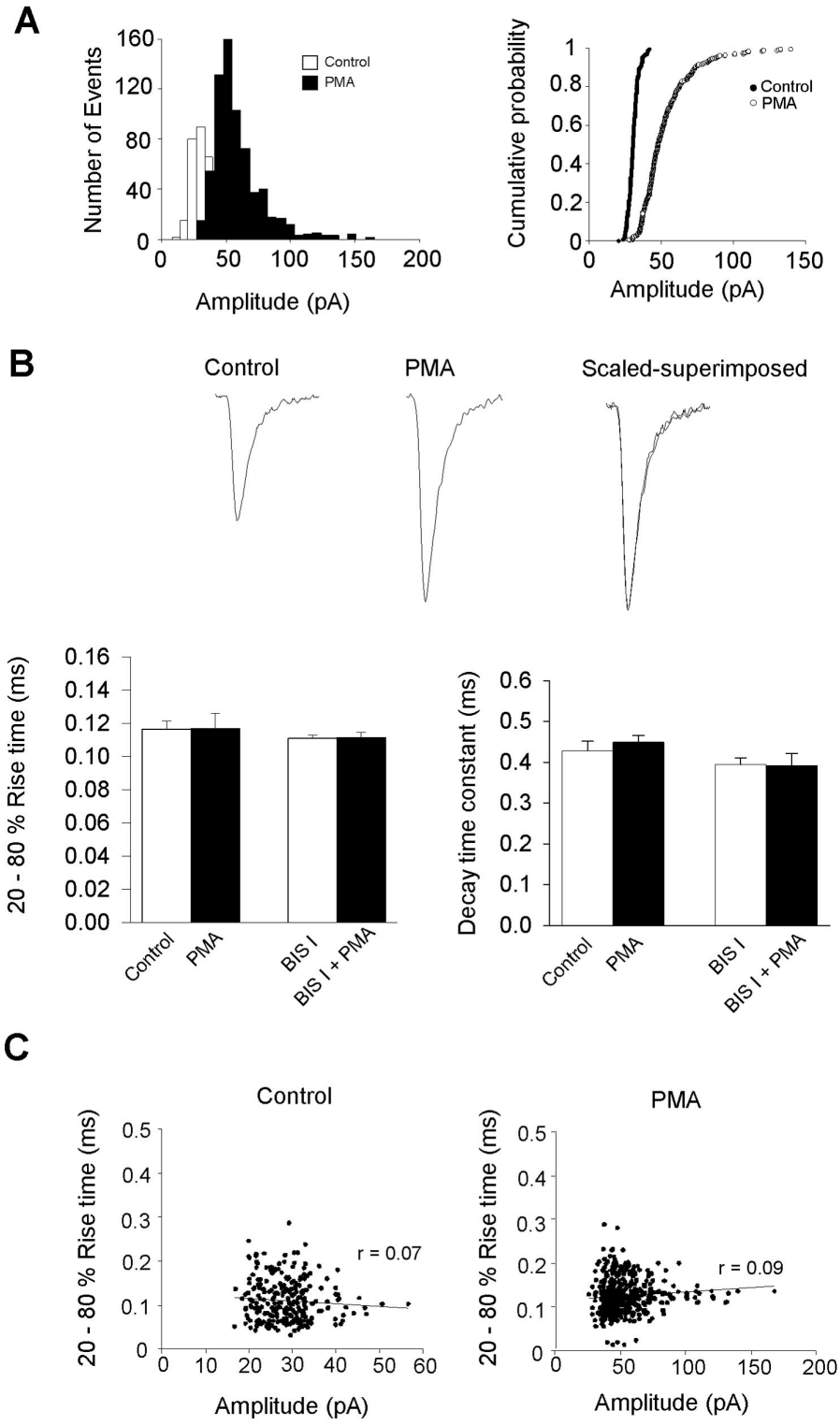

Fig. S1. PMA-induced increase in mEPSC amplitude is not due to changes in kinetics or dendritic filtering. (*A*) Amplitude histogram of mEPSCs from a Mauthner cell recorded before (control; open squares) and after PMA (closed squares) application (binwidth = 2 pA; $n = 263$ (control); $n = 756$ (PMA) (*Left*). PMA significantly shifts the cumulative probability plot of the mEPSCs amplitude (*Right*). (*B*) Representative traces of mEPSCs (*Left*, control; *Center*, PMA) from the same cell before and after PMA application. When scaled and superimposed (*Right*), the traces do not differ in their time courses and kinetics. Bar graphs of the 20–80% rise time and the decay time constants of the mEPSC indicate that there is no change in kinetics after application of PMA. Error bars indicate mean ± SEM. (*C*) Scatter plot of rise time vs. amplitude of events recorded before and after application of PMA. There was no correlation between these parameters before or after PMA application (*Left*, control: $r = 0.07$; *Right*, PMA-enhanced mEPSCs: $r = 0.09$).

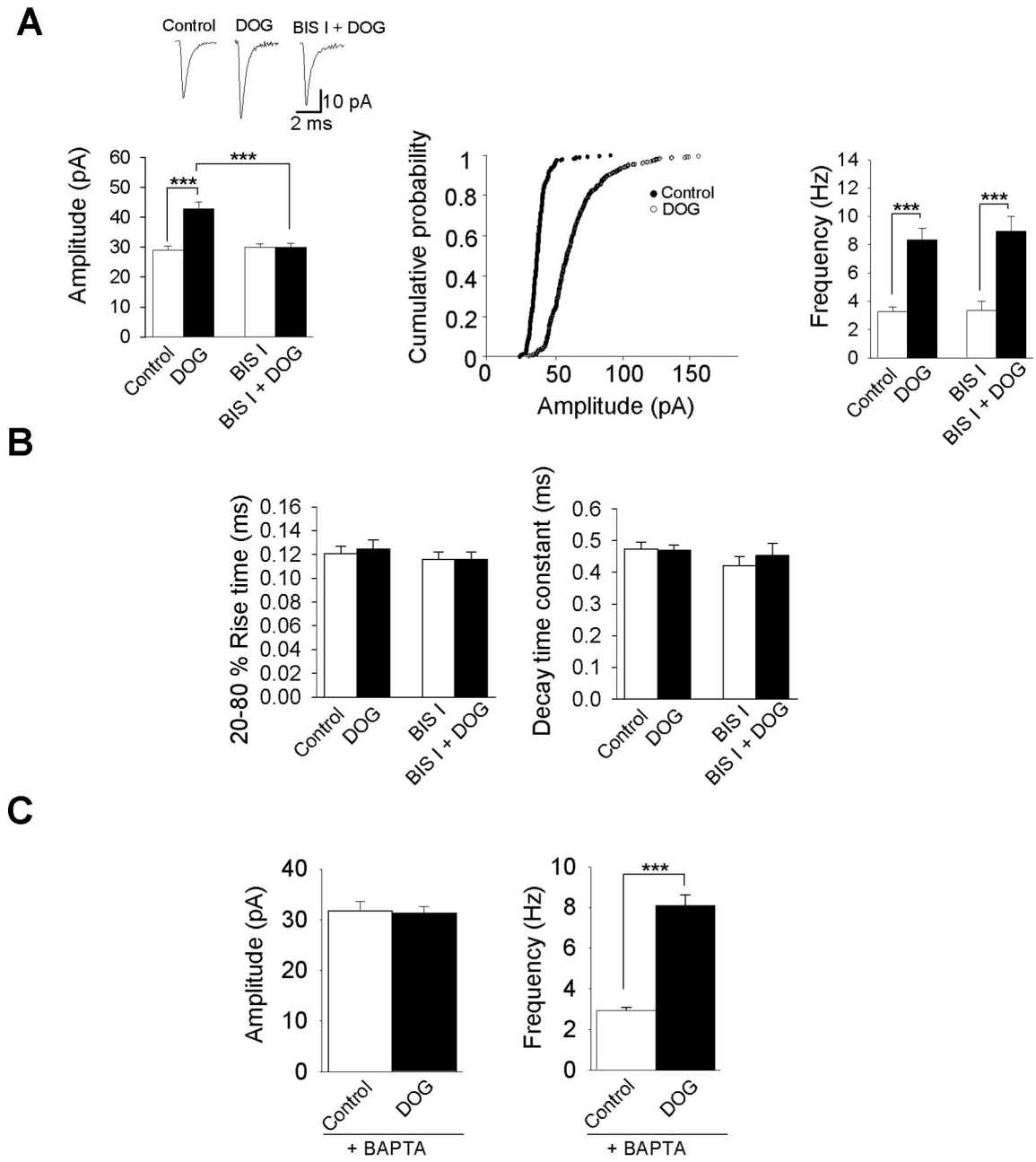

Fig. S2. DOG-induced increase in mEPSC amplitude is not due to changes in kinetics or dendritic filtering. (*A*) Bath application of the DAG analog 1,2-dioctanoylglycerol (DOG, 50 μM) increased the mean mEPSC amplitude (*Left*) and frequency (*Right*) ($n = 5$, $P < 0.001$). DOG significantly shifts the cumulative probability plot of the mEPSCs amplitude (*Center*). Intracellular application of BIS I (500 nM; $n = 5$), before DOG application, blocked the increase in amplitude but did not affect the mean mEPSC frequency. (*B*) Bar graphs of the 20–80% rise time and the decay time constants of the mEPSC indicate that there is no change in kinetics following application of DOG. (*C*) Preventing the rise in intracellular Ca^{2+} by including BAPTA (5 mM) in the patch pipette blocked the DOG-induced increase in amplitude ($n = 5$, $P < 0.001$), but had no effect on the mEPSC frequency. Error bars indicate mean ± SEM. ***, significantly different, $P < 0.001$.

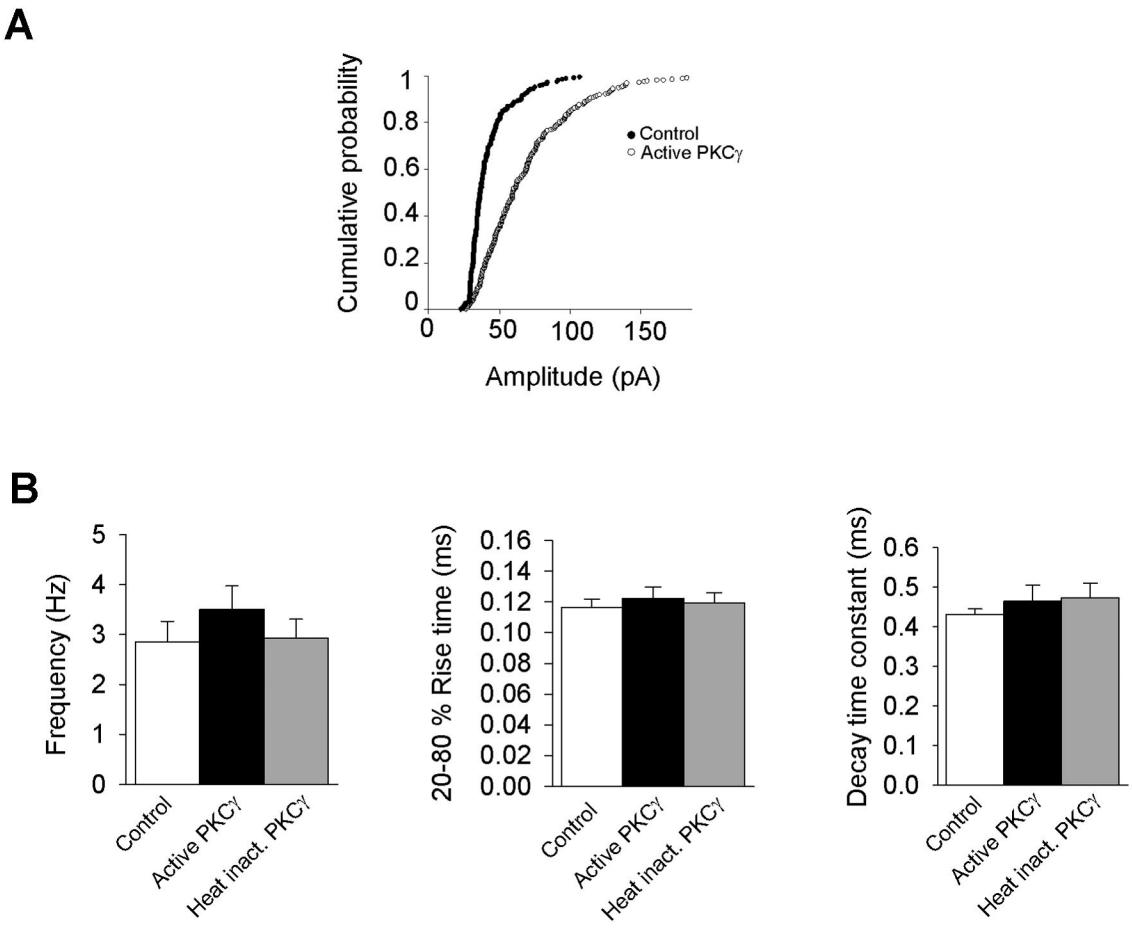

Fig. S3. Active PKCγ does not change mEPSC kinetics. (*A*) Active PKCγ significantly shifts the cumulative probability plot of the mEPSCs amplitude. (*B*) Application of active and heat inactivated PKCγ had no effect on mEPSC frequency, 20–80% rise time or decay time constant. Error bars indicate mean ± SEM.

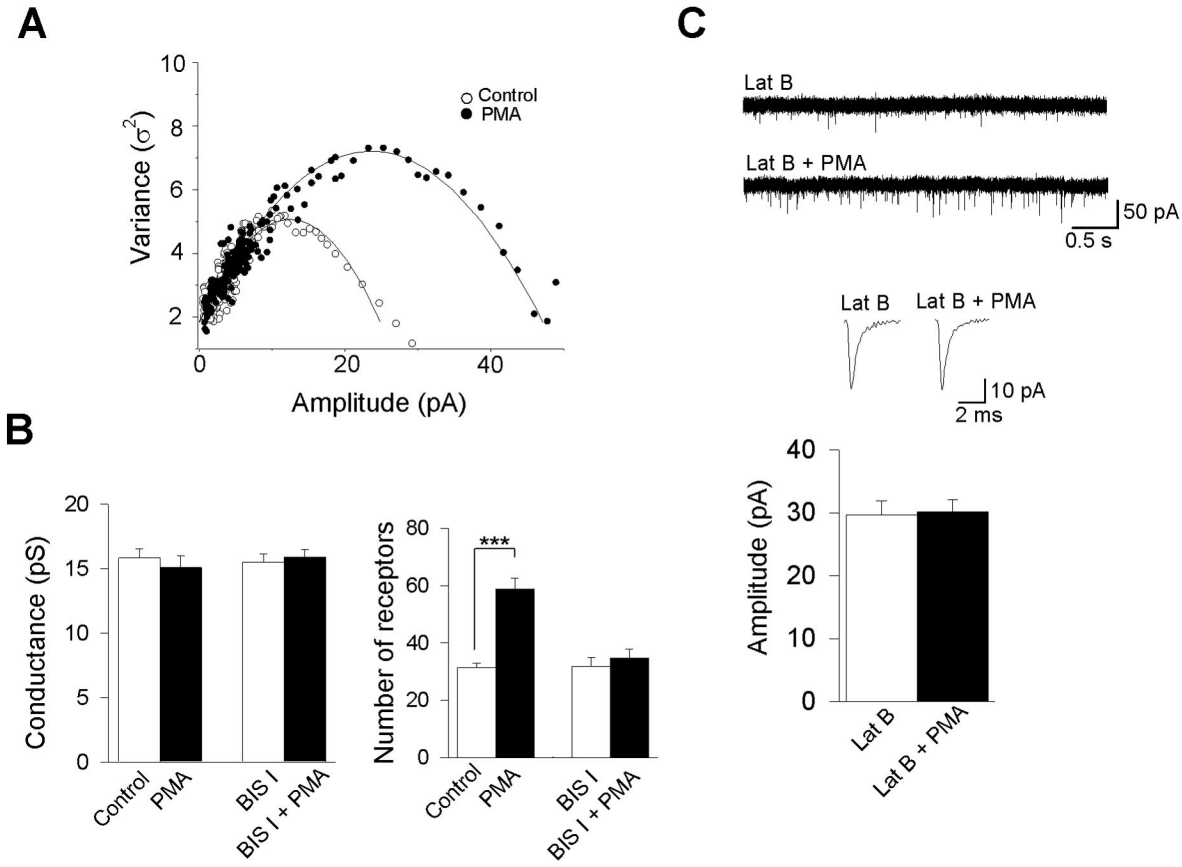

Fig. S4. NSFA indicates that the PMA-induced increase in mEPSC amplitude is due to receptor trafficking. (*A*) Plot of variance vs. mean current of mEPSCs before (open circles) and after application of PMA (solid circles). The parabolic curves exhibited overlap over the initial linear portion and large increases in the variance. (*B*) PMA did not change the unit conductance ($n = 7$), but it increased the number of functional postsynaptic AMPARs ($n = 7$, $P < 0.001$). Intracellular application of BIS I blocked the effect of PMA ($n = 6$, $P = 0.659$). (*C*) Effect of latrunculin B (Lat B, 5 mM) on mEPSCs recorded before and after application of PMA (100 nM). Latrunculin B significantly blocked the effect of PMA on the amplitude ($n = 5$). Error bars indicate mean ± SEM. ***, significantly different, $P < 0.001$.

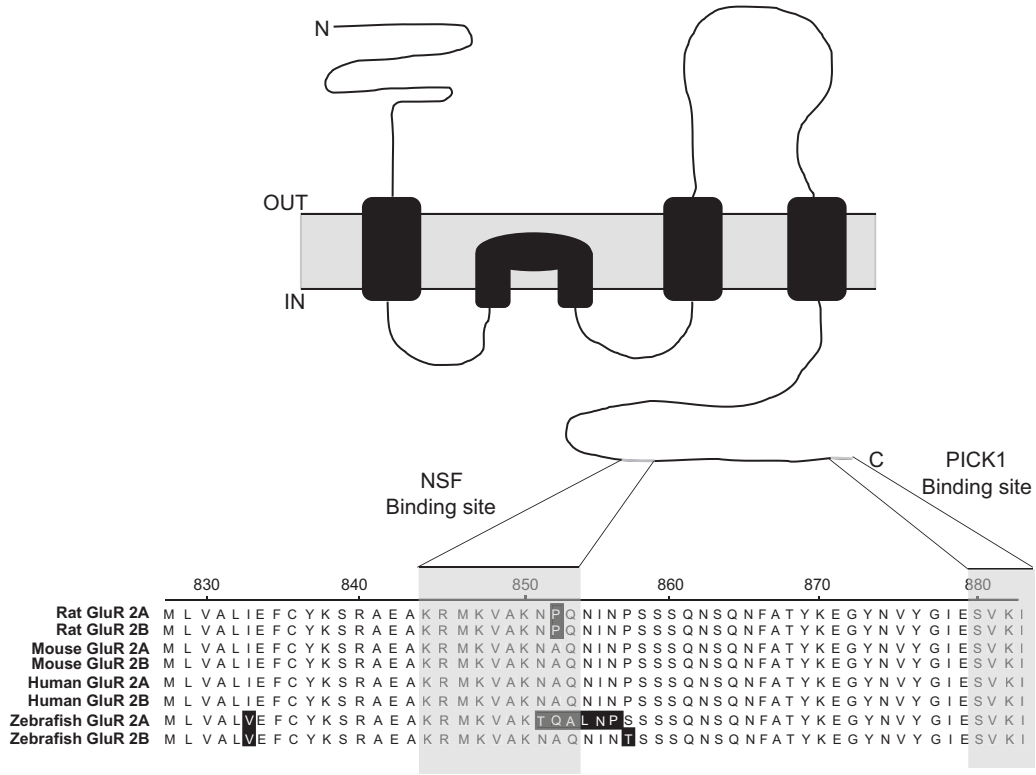

Fig. S5. Sequence alignment of the C terminus of the GluR2 subunit. The last ≈55 aa at the C terminus of the zebrafish GluR2A and B, rat, mouse and human GluR2 isoforms were aligned by Clustal W. Residues that are not conserved are indicated in black. Binding sites for NSF and PICK1 are boxed.

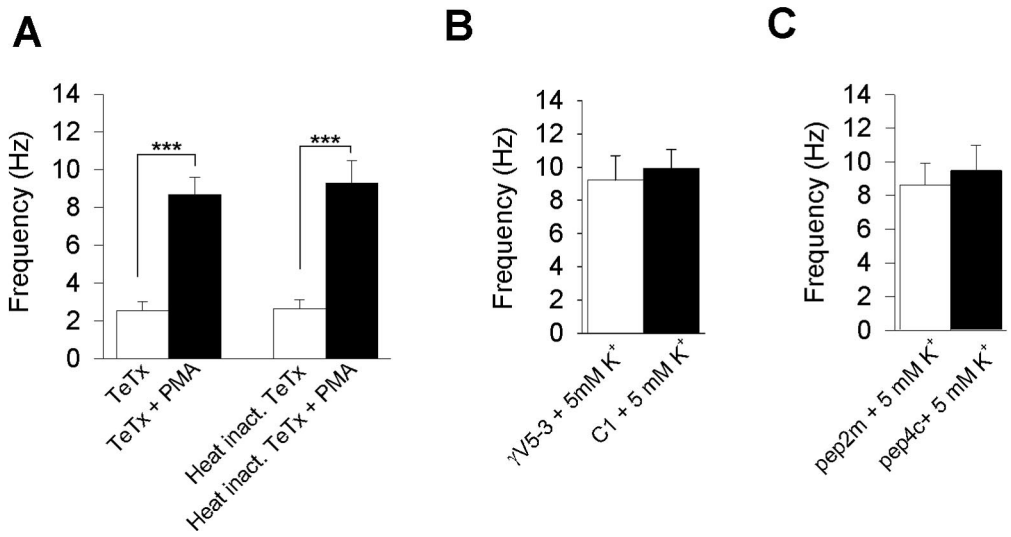

Fig. S6. TeTx, V5–3γ and pep2M do not have presynaptic effects. (*A*) Intracellular application of TeTx (200 nM; $n = 6$) or heat-inactived TeTx ($n = 4$) had no effect on the PMA-induced increase in mEPSC frequency. (*B*) Inclusion of either γV5–3 (10 nM; $n = 5$) or the control peptide (C1; 10 nM) ($n = 5$) in the patch pipette had no effect on the 5 mM K^+ induced increase in mEPSC frequency. (*C*) Application of pep2m (200 μM, $n = 5$) or pep4c (200 μM, $n = 5$) in the recording solution had no effect the 5 mM K^+ induced increase in mEPSC frequency. Error bars indicate mean $\pm$ SEM.

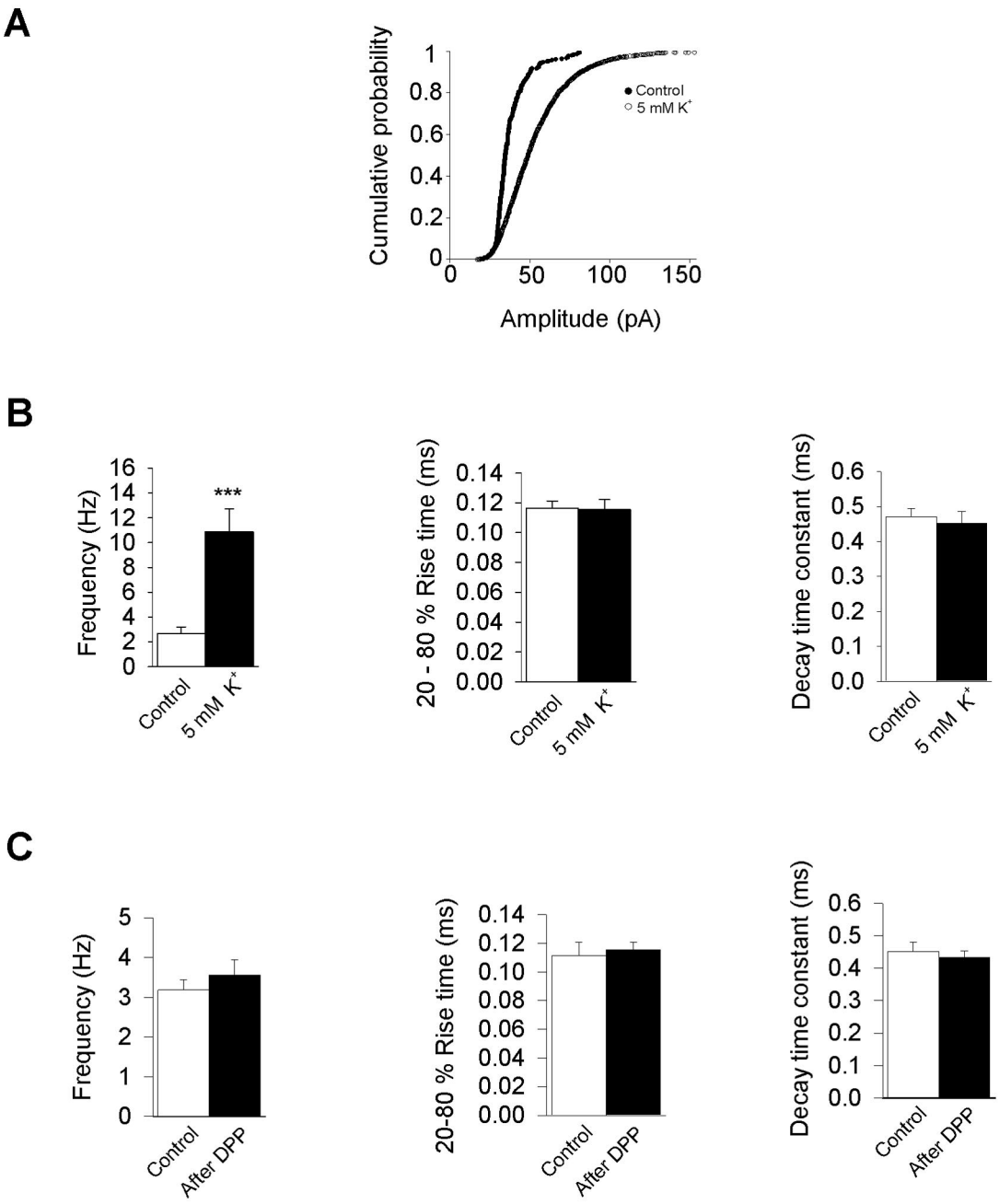

Fig. S7. Application of 5 mM K^+ or a depolarization protocol (DPP) does not affect mEPSC kinetics. (*A*) Application of the 5 mM K^+ medium shifts the cumulative probability plot of the mEPSCs amplitude. (*B*) Application of the 5 mM K^+ solution for 10 min significantly increased mEPSC frequency, but did not alter the rise time and the decay time constant of the mEPSCs ($n = 6$). (*C*) Bar graphs of the mEPSC frequency, 20–80% rise time and the decay time constant of the mEPSC indicate that there is no change in these parameters after the depolarizing pulse protocol (DPP) ($n = 5$). Error bars indicate mean ± SEM.

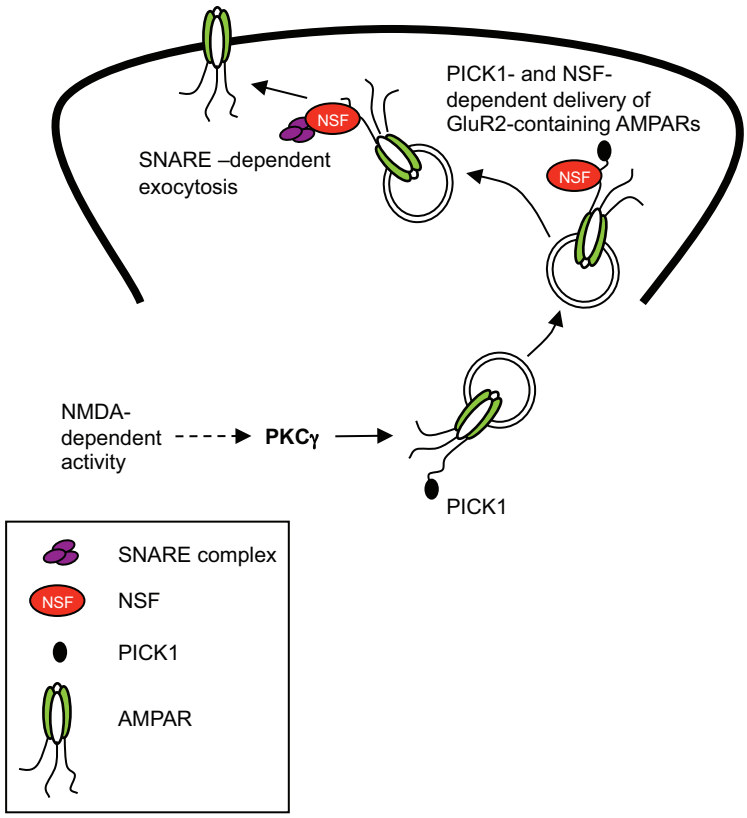

Fig. S8. Proposed model for trafficking of AMPAR in embryonic zebrafish Mauthner cell. An increase in NMDA-dependent cellular activity leads to the activation of PKCγ, which recruits PICK1 to the C terminus of the GluR2 subunit. AMPARs are trafficked to the membrane where association with NSF and SNARE proteins lead to their insertion into the membrane.